the probable instability of the small-scale flow features sustained by the transfer of energy from the large scales, is the stretching of vorticity caused by the external straining of the free shear layers and the shock waves in this transonic flow. This mechanism is expressed by the vorticity equation for compressible nonisentropic flow

$$\frac{D}{Dt}\frac{\omega}{\rho} = \frac{\omega}{\rho}\cdot E + \frac{1}{\rho^3}(\text{grad } \rho \times \text{grad } p)$$

where $E$ is the rate-of-strain tensor.

The aim then is to test this hypothesis in a numerical experiment simulating a flow where the term $(\omega/\rho)\cdot E$ is large. This is feasible because the stretching and distorting of the primary vortex can be accentuated by the geometrical shape of the wing. Consider flow past a cropped delta whose leading edge is not a straight line nor does it even lie in a plane—a so-called cranked-and-cropped delta wing with twist. The core of the vortex generated by the leading edge inboard of the crank will not be straight, and its velocity field will strain the leading-edge vortex starting outboard of the crank. The simulated flow for $M_\infty = 0.9$ $\alpha = 8$ deg using a grid of $193 \times 57 \times 97$ nodes is displayed in Figs. 2. The first of these figures gives a schematic representation of the main discernible features in the isoMach lines on the upper surface of the wing. Inboard of the crank a leading-edge shock wave interacts with the primary vortex, while further aft the flow is rather smooth except for a shock and a shear line.

Outboard of the crank and shear line, it changes dramatically. The different leading-edge sweep causes the inboard vortex to degenerate from a well-ordered feature into many smaller-scale eddies with substantial transient frequencies. The mechanism for this physical flow instability is, we believe, the stretching of the vortex produced at the crank. Outboard of the crank, another shock and vortex appear along the leading edge. This vortex then runs into the side edge of the cropped tip, turns because of the shear flow separating from the edge, and degenerates into small eddies. The overall flow pattern suggests, qualitatively at least, the presence of large-scale coherent turbulence. This particular wing exists only as numbers in the computer; we have no measurements to compare with and therefore cannot yet assess the quantitative realism of the simulation. The integrated values of lift and drag, $C_L = 0.466$ and $C_D = 0.059$ are quite reasonable. Comparison of the flow simulated after 1000 time steps and 2000 time steps indicates that these values change very little and that the flow is at least statistically steady. The small eddies meander around the upper surface but not out of the flowfield. These first results seem to support the hypothesis of energy transfer to small scales by vortex stretching.

The turbulentlike character occurs not only on the wing surface but out in the field as well. The isobars in three chordwise surfaces (Fig. 2e) confirm the trend from laminar to turbulent flow. The highly compressible nature of this case is evident around the leading edge. It seems that the shock waves at the leading edge produce entropy layers that are shed into the field over the wing. This layer is reasonably thin, but Fig. 2f reveals its unstable wavelike character in the spanwise direction from the crank to the tip.

## References

[1]Rizzi, A., "Modelling Vortex Flowfields by Supercomputers with Super-size Memory," *Aeronautical Journal,* April 1985, pp. 149-161.

[2]Eriksson, L.E., "Generation of Boundary-Conforming Grids Around Wing-Body Configurations Using Transfinite Interpolation," *AIAA Journal*, Vol. 20, Oct. 1982, pp. 1313-1320.

[3]Rizzi, A.W. and Eriksson, L.E., "Computation of Flow Around Wings Based on the Euler Equations," *Journal of Fluid Mechanics*, Vol. 148, Nov. 1984, pp. 45-71.

# Application of Steady Shock Polars to Unsteady Shock Wave Reflections

G. Ben-Dor*
*Ben-Gurion University of the Negev*
*Beer Sheva, Israel*
and
K. Takayama†
*Tohoku University, Sendai, Japan*

IN the course of the present study, an experimental investigation of the dynamics of the MR→RR transition over concave cylinders was performed. It was found that the process goes through the following sequence of events: direct Mach reflection → stationary Mach reflection → inverse Mach reflection and finally transition to regular reflection. Furthermore, it is shown that the steady $(P,\theta)$ shock polars can be used in a special way to understand the transition process and also to explain the resulted wave configuration.

The present experimental study brings more light and understanding to this complex transition phenomenon over a concave cylinder. It is hoped that the present study will be of help to investigators interested in establishing the analytical transition criterion for this reflection phenomenon.

## Present Study

Figure 1 illustrates the triple-point trajectory of the Mach reflection over the the concave cylinder. The experimental results indicate that the length of the Mach stem $\lambda$ increases from $\lambda = 0$ to a maximum, after which it decreases until it vanishes ($\lambda = 0$) at the point where transition to regular reflection takes place. It should be noted that the first measured data point is not at the beginning of the cylindrical wedge; however, since $\lambda$ must start from zero, a reasonable trajectory is drawn in dashed lines in the region where experimental data are unavailable. Consequently, the triple-point trajectory can be divided into two parts; a part in which $d\lambda/ds > 0$ and a part in which $d\lambda/ds < 0$, where $s$ is a distance measured along the wedge surface.

Courant and Friedrichs[1] introduced three different types of Mach reflection depending upon whether the triple point moves away from, parallel to, or toward the reflecting wedge. These three different types of Mach reflection, which were termed by them direct Mach, stationary Mach, and inverse Mach reflections, are shown schematically in Fig. 2 as inserts A, B, and C, respectively.

Following Courant and Friedrichs,[1] one can conclude that the experimental measurement of the triple-point trajectory (Fig. 1) suggests that the reflection of a planar shock wave over a concave cylinder goes through the following sequence of events: a direct Mach reflection along the part where $d\lambda/ds > 0$, a stationary Mach reflection at the point where $d\lambda/ds = 0$, an inverse Mach reflection along the part where $d\lambda/ds < 0$, and finally a regular reflection after the point where the MR→RR transition occurs.

In order to get a better insight into this phenomenon, it was decided to divide the truly unsteady flow into a sequence of momentarily pseudosteady flows and to use the steady $(P,\theta)$ polars. Although the use of steady $(P,\theta)$ polars for truly

Received Feb. 28, 1984; revision received July 12, 1985. 

*Associate Professor, Department of Mechanical Engineering.
†Associate Professor, Institute of High Speed Mechanics.

unsteady flows is not fully justified, it will be shown that much can be learned from the steady $(P,\theta)$ polars about the dynamics of the transition. Consequently, we believe that the steady $(P,\theta)$ polars can be used for at least explanatory purposes and basic understanding of truly unsteady phenomenon. It is of interest to note that Marconi[2] used shock polars in his study of the RR ⇔ MR transition in steady three-dimensional flows. The third dimension in his study might be considered as similar to the time dimension in two-dimensional unsteady flows.

A multishock polar diagram is shown in Fig. 2. When the incident shock wave propagates along the wedge, its Mach number remains constant. However, the effective wedge angle $\theta_w$ increases and hence the oncoming flow Mach number $M_0$ with respect to the triple point increases. Thus, for a given location of the incident shock wave on the curved cylinder, the momentary value of $M_0$ can be calculated and, hence, the corresponding momentary pseudosteady shock polar can be drawn. Three combinations of *I-R* polars are shown in Fig. 2. Since the incident shock wave moves at a constant velocity, the pressure jump across it remains constant. Therefore, all the *R* polars emanate from their corresponding *I* polars at the same pressure. Figure 2 shows a direct Mach reflection at point a (the $I_1$ and $R_1$ polar intersection is on the right portion of the $I_1$ polar), a stationary Mach reflection at point b (the $I_2$ and $R_2$ polar intersection is on the *P* axis), an inverse Mach reflection at point c (the $I_3$ and $R_3$ polar intersection is on the left portion of the $I_3$ polar), and finally a regular reflection at point d (the intersection of the $R_3$ polar with the *P* axis). Consequently, the process goes through the following sequence of events: direct Mach reflections from point a along the dashed line up to point b where a momentary stationary Mach reflection is obtained. This stationary Mach reflection immediately changes into an inverse Mach reflection. Then the inverse Mach reflection is maintained along the dashed line between points b and c. Then, a sudden transition from an inverse Mach reflection at point c to a regular reflection at point d takes place. Note that the multishock polar diagram suggests that when the inverse Mach reflection terminates (point c) and the regular reflection forms (point d), the pressure drops from $P_c$ to $P_d$. According to Henderson and Lozzi,[3] "If a pressure discontinuity occurs during transition then an unsteady wave of finite amplitude or a finite amplitude band of waves will be generated in the flow." We may therefore expect that, since the transition is associated with a pressure drop, the regular reflection will be followed by either compression waves or a shock wave supporting the sudden pressure drop. As will be shown in the present case, a shock wave supports this sudden pressure drop. The fact that this additional shock wave, suggested by the multishock polar technique, indeed appears in the MR→RR transition over concave cylinders supports the

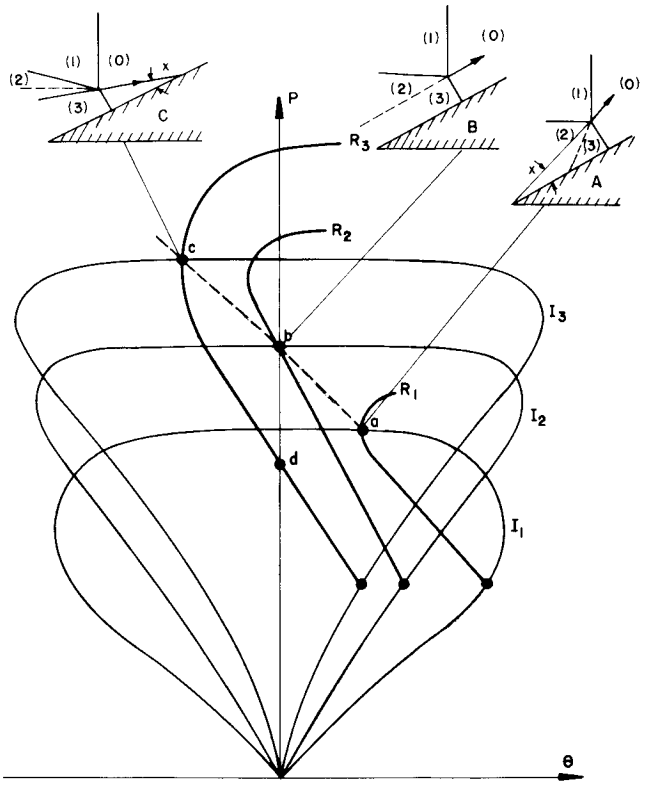


**Fig. 2 Multi-shock polar diagram of the reflection process described in Fig. 1: a) direct-Mach reflection; b) stationary-Mach reflection; c) inverse-Mach reflection; d) regular reflection. (The dashed line illustrates the reflection process.)**

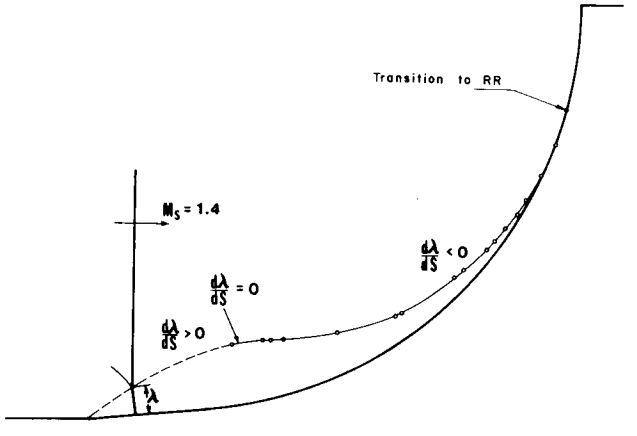


**Fig. 1 Experimental data of the triple point trajectory of an incidental shock wave $M_s = 1.4$ propagating over a cylindrical concave wedge having a radius of curvature $R = 50$ mm.**

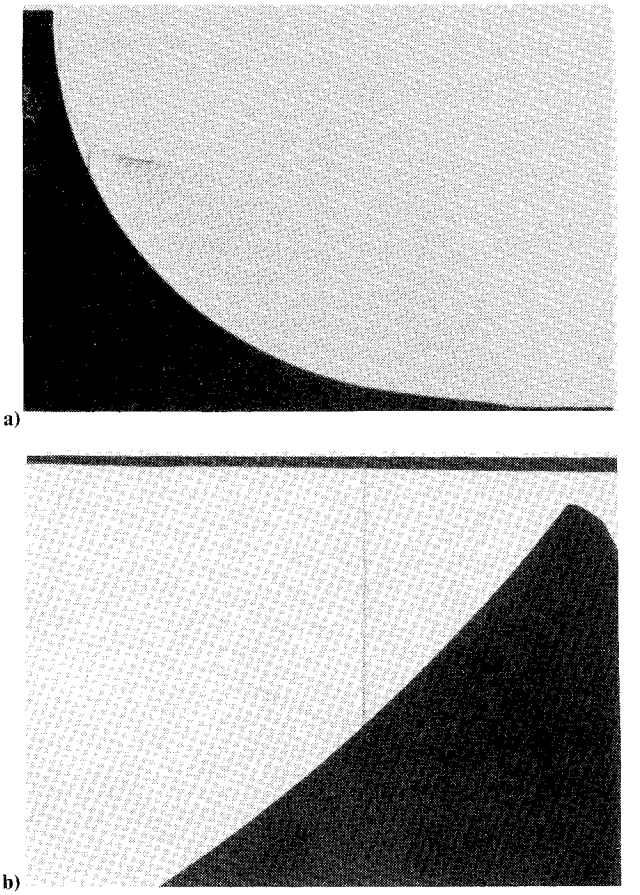


**Fig 3 Shadowgraph illustrating the regular reflection which is formed after the termination of the inverse-Mach reflection: a) strong incident shock wave; b) weak incident shock wave.**

justification of the use of steady shock polars for a better understanding of truly unsteady flows and for explanatory purposes.

Figure 3a illustrates the regular reflection after transition. The incident shock wave is reflected regularly from the wedge surface. Behind the point of reflection the additional shock wave, which was mentioned earlier, can clearly be seen. The existence of this shock wave was suggested by the multishock polar technique. Its purpose is to support the sudden pressure drop from $P_c$ to $P_d$ (Fig. 2) that takes place at transition. Note that the additional shock wave forms a new triple point on the reflected shock wave of the regular reflection. The slipstream of this triple point collides with the wedge surface and reflects from it in a way which can be termed as "regular reflection of a slipstream." The foregoing discussion concerning the role of the additional shock wave suggests that its strength should be in the vicinity of $P_c/P_d$. Figure 3b illustrates a regular reflection (which was formed after the termination of the inverse Mach reflection) of a *weak* incident shock wave. The above-mentioned additional shock wave is again clearly seen. However, the slipstream emanating from the triple point is probably too weak to be noticed with shadowgraph photography.

## Conclusions

The transition from Mach to regular reflection over a concave cylinder was investigated experimentally. The steady flow $(P,\theta)$ shock polars were used for this unsteady phenomenon in a special way to better understand the process. Although they were used in a truly unsteady flow, it was found that they can predict the phenomenon quite accurately. The use of the multishock polar technique suggested that the transition should go through an inverse Mach reflection and that an additional shock wave should appear after transition to regular reflection behind the reflection point. Both of these predictions were verified experimentally. The experimental study also illustrated the dynamics of the transition from Mach to regular reflection over concave cylinders. Further details on the nature of the inverse Mach reflection can be found in Ref. 4.

## References

[1]Courant, R. and Friedrichs, K.O., *Supersonic Flow and Shock Waves*, Vol. 1, Interscience Publications Inc., New York, London, 1948.

[2]Marconi, F., "Shock Reflection Transition in Three-Dimensional Steady Flow About Interfering Bodies," *AIAA Journal*, Vol. 21, May 1983, pp. 707-713.

[3]Henderson, L.F. and Lozzi, A., "Experiments on Transition of Mach Reflections," *Journal of Fluid Mechanics*, Vol. 68, Pt. 1, March 1975, pp. 139-155.

[4]Takayama, K. and Ben-Dor, G., "The Inverse Mach Reflection," *AIAA Journal*, Vol. 23, Dec. 1985, pp. 1853-1859.

# Visualization of a Forced Elliptic Jet

Ephraim Gutmark* and Chih-Ming Ho†
*University of Southern California*
*Los Angeles, California*

## Introduction

COHERENT structures have been recognized as the dominating feature in free shear layer dynamics.[1-3] Extensive measurements and visualizations have been made about the structures in a circular jet. Recently, Ho and Gutmark[4] found that an elliptical jet with a small aspect ratio (2:1) could substantially increase the entrainment and hence suggested that jets with a small-aspect-ratio asymmetric nozzle could be *an effective passive enhancement device* for entrainment. However, the evolution of elliptical coherent structures are practically unknown, although data about an isolated vortex ring[5,6] or rectangular jet[7,8] with an aspect ratio larger than 5:1 have been reported.

The visualization of coherent structures in an elliptic jet forced in a wide frequency range was presented by the authors at two meetings.[4,9] This range consisted of $1.5\ f_i \geq f_F \geq 0.33\ f_i$, where $f_F$ is the forcing frequency and $f_i$ the initial most amplified frequency in an unforced jet. The evolution of elliptical structures forced at two chosen frequencies is documented in this brief Note. At a low forcing frequency ($f_F = 0.45\ f_i < \frac{1}{2} f_i$), the vortex merging did not occur before the end of the potential core. The vortex merging could be observed about the middle of the potential core at the higher forcing frequency ($f_F = 0.65\ f_i > \frac{1}{2} f_i$).

## Facility

The flow visualization was carried out in an elliptic water jet submerged in a water tank ($737 \times 737 \times 1219$ mm$^3$). The jet had an elliptic nozzle with major and minor diameters of 50.8 mm ($2a$) and 25.4 mm ($2b$), respectively. The shape of the contraction section was circular at the stagnation chamber side and elliptic at the exit. The contours of the contraction in both axis planes were fifth-order polynomials. The diameter of the stagnation chamber was 127 mm. The area contraction ratio was 12.5:1. Honeycomb and screens were installed inside the stagnation chamber to reduce the turbulence level. The water jet was driven by a water pump at a Reynolds number of 14,000, based on the nozzle's major diameter and the exit velocity $U_j$. Forcing was applied by a rotating butterfly valve, which was installed in the bypass branch of the water supply. The initial most amplified frequency $f_i$ in the unforced jet was 6 Hz. The forcing amplitude was about 5% of the jet exit speed. Food color was injected uniformly around the nozzle lip so that the entire vortex ring could be visualized.

## Experimental Results

In the elliptic jet forced at high amplitude $0.05U_j$, the coherent structures were formed at the forcing frequency. Figure 1a shows the flow for the condition $f_F = 0.45\ f_i$, in the view of the major axis plane (the plane containing the major axis of the nozzle). At this forcing frequency, vortices did not merge before the end of the potential core, $x = 5a$. Two features, the lateral deformation and the bending, were distinct from the evolution of the structures in a circular jet. After the vortex ring left the nozzle, it shrank and then expanded in the lateral direction. The necking of the jet column occurred at $x \simeq 1.5a$. The view in the minor axis plane (Fig. 1b) revealed that the structure first expanded and then shrank. Therefore, the elliptic vortex ring switched its axis at $x \simeq 1.5a$ and again at $x \simeq 3a$. Bending of the vortex in the two axis planes were in opposite directions and reached a maximum at $x \simeq a$. The ring became almost flat at $x \simeq 1.5a$ (Fig. 1b). These distortions of nonmerging structures in a jet were very similar to those of an isolated elliptic vortex.[5,6] The measured width $w$ in both axis planes and the maximum deflection $H$ (Fig. 2) agreed well with the numerical results of a single vortex.[6] Obviously, the dynamics of these two flows should be different. However, the matching of the shape distortions implies that the same mechanism, self-induction, governs the deformation of an isolated elliptic vortex[5,6] and the deformation of structures in an elliptic jet.

When the jet was forced at a higher frequency, $f_F = 0.65\ f_i$, vortex merging before the end of the potential core was observed (Fig. 3). Upstream from the merging, the vortices bent and distorted in the lateral direction. However, the defor-

Received April 6, 1984; revision submitted May 24, 1985. 

*Research Associate.
†Professor. Member AIAA.